Molecular Basis of Sulfonylurea Herbicide Inhibition of Acetohydroxyacid Synthase*

Siew Siew Pang, Luke W. Guddat, and Ronald G. Duggleby‡

From the Department of Biochemistry and Molecular Biology, The University of Queensland, Brisbane QLD 4072, Australia

Acetohydroxyacid synthase (AHAS) (acetolactate synthase, EC 4.1.3.18) catalyzes the first step in branched-chain amino acid biosynthesis and is the target for sulfonylurea and imidazolinone herbicides. These compounds are potent and selective inhibitors, but their binding site on AHAS has not been elucidated. Here we report the 2.8 Å resolution crystal structure of yeast AHAS in complex with a sulfonylurea herbicide, chlorimuron ethyl. The inhibitor, which has a K_i of 3.3 nM, blocks access to the active site and contacts multiple residues where mutation results in herbicide resistance. The structure provides a starting point for the rational design of further herbicidal compounds.

Herbicides are widely used for weed control in agriculture and industry and are also used by government agencies and home gardeners. It is estimated that worldwide sales of herbicides exceed $30 billion, with the sulfonylureas (Fig. 1*a*) and imidazolinones (Fig. 1*b*) accounting for about $2 billion in annual sales. The sulfonylureas and imidazolinones act by preventing branched-chain amino acid biosynthesis by virtue of their specific and potent inhibition of acetohydroxyacid synthase (AHAS)[1] (acetolactate synthase, EC 4.1.3.18), the first enzyme in this pathway (1, 2).

AHAS catalyzes the decarboxylation of pyruvate and its combination with another 2-ketoacid to give an acetohydroxyacid (3, 4). The enzyme requires three cofactors: thiamine diphosphate (ThDP), a divalent metal ion such as Mg^{2+}, and FAD. The requirement for the first two of these cofactors is well understood from the chemistry of ThDP and the three-dimensional structure of various enzymes including AHAS (5) and its relatives pyruvate oxidase (6), pyruvate decarboxylase (7, 8), and benzoylformate decarboxylase (9). In contrast, the role of FAD remains puzzling, despite now knowing the location and conformation of this cofactor in the enzyme (5).

The herbicides that inhibit AHAS bear no resemblance to the substrates and are not competitive inhibitors, suggesting that they bind at a site distinct from the active site (1, 10–13).

---

‡ To whom correspondence should be addressed: Dept. of Biochemistry and Molecular Biology, The University of Queensland, Coopers Rd., St. Lucia, Brisbane QLD 4072, Australia. Tel.: 61-7-3365-4615; Fax: 61-7-3365-4699; E-mail: Ronald.Duggleby@mailbox.uq.edu.au.

[1] The abbreviations used are: AHAS, acetohydroxyacid synthase; CE, chlorimuron ethyl; FAD, flavin adenine dinucleotide; ThDP, thiamine diphosphate.

Previously, we proposed (5) a model for the herbicide-binding site, based on the structure of yeast AHAS and the location of residues where mutation is known to result in herbicide insensitivity. However, this site is large and exposed to solvent, and we suggested that structural changes would occur upon binding of substrates or herbicides. In this paper, we describe the crystal structure of yeast AHAS in complex with chlorimuron ethyl (CE; Fig. 1*a*), a commonly used sulfonylurea herbicide. Our structure provides the first view of the mode of binding between an herbicidal inhibitor and AHAS and elucidates the location of the herbicide resistance mutations in this enzyme.

EXPERIMENTAL PROCEDURES

Expression, Purification, Crystallization, and X-ray Data Collection—The catalytic subunit of yeast AHAS was expressed and purified as described previously (14). Crystals of yeast AHAS were grown by hanging drop vapor diffusion in the presence of 1 mM ThDP, 1 mM $MgCl_2$, 1 mM FAD, 1 mM CE, 5 mM dithiothreitol, 0.2 M potassium phosphate, pH 7.0, 0.1 M Tris-HCl, pH 7.0, 0.2 M Li_2SO_4, and 0.9 M sodium potassium tartrate. X-ray data (Table I) were collected from cryoprotected crystals (30% v/v ethylene glycol) at 100 K on Beam Line 14D at the Advanced Photon Source in the Argonne National Laboratory (Chicago, IL). The data were indexed, integrated, and scaled using the programs DENZO and SCALEPACK (15).

Structure Determination—The crystal structure was solved by molecular replacement using the program AMoRe (16), starting with our previous yeast AHAS structure (Ref. 5; Protein Data Bank accession number 1JSC) as the search model. Rigid body refinement with the CNS software package (17) reduced the R_{factor} from 0.476 to 0.424 for data from 6.0 to 2.8 Å resolution. The structural models were checked against the initial 2.8 Å resolution $2F_o$-F_c and F_o-F_c electron density maps using the program O (18). Even at the earliest stage of refinement, there was well-defined electron density for both CE and the capping region that will be described later. During all stages of refinement, tight noncrystallographic symmetry restraints were applied to the core regions. Individual *B*-factors were assigned for all atoms, and an overall anisotropic *B*-factor correction was applied using the standard protocol in the CNS software package. As well as the two polypeptide structures, 2 FAD molecules, 2 ThDP molecules (1 partially degraded, see below), 2 Mg^{2+}, 2 K^+, 2 dithiothreitol molecules, 2 CE molecules, and 832 ordered water molecules were observed in each asymmetric unit. The R_{factor} and R_{free} for the final structure are 0.163 and 0.205, respectively, and the model has excellent geometry (Table I). The coordinates and structure factors of the yeast AHAS·CE complex have been deposited with the Research Collaboratory for Structural Bioinformatics Protein Data Bank (accession number 1N0H). Figures were generated with LIGPLOT (19), SETOR (20), MOLSCRIPT (21), RASTER 3D (22), WebLab ViewerPro (MSI, San Diego, CA), and INSIGHT2001 (Accelrys).

Mutagenesis, Assay, and Herbicide Inhibition—Mutations were introduced by PCR using the megaprimer method (23). AHAS activity and inhibition constants for imidazolinones and sulfonylureas were determined using methods described previously (24, 25).

RESULTS AND DISCUSSION

Overall Structure of the AHAS·CE Complex—Yeast AHAS was co-crystallized with a sulfonylurea herbicide (CE), and the structure was solved by molecular replacement using the free
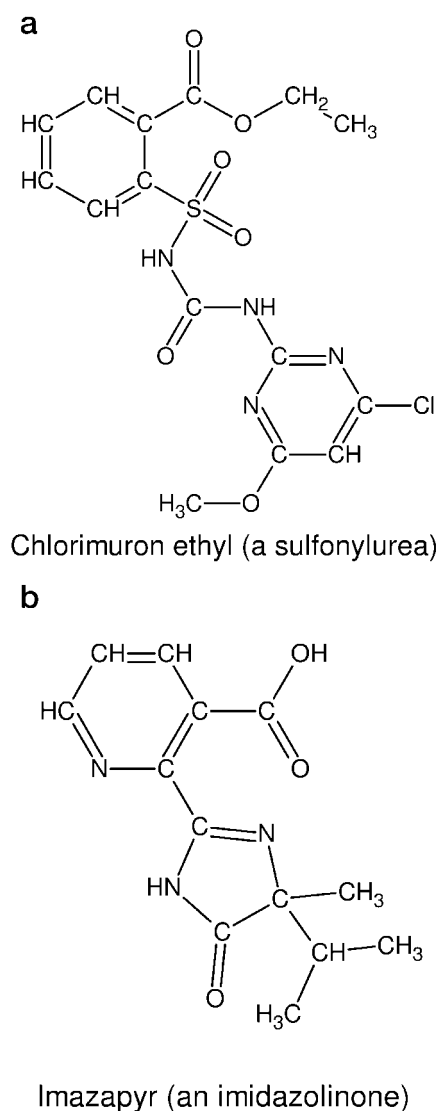
a

Chlorimuron ethyl (a sulfonylurea)

b

Imazapyr (an imidazolinone)

FIG. 1. **The chemical structures of:** *a*, CE, a sulfonylurea herbicide; and *b*, imazapyr, an imidazolinone.

enzyme (5) as the starting model. The AHAS·CE complex has an overall fold that is similar to that of the free enzyme with the subunits tightly associated by virtue of numerous noncovalent interactions across the dimer interface. Each of the two monomers (referred to as A and B) is folded into three domains of approximately equal size (Fig. 2*a*), designated as α (residues 85–269), β (residues 281–458), and γ (residues 473–643). The surfaces of the α- and γ-domains in each monomer form the subunit interface, whereas the β-domains are distal to each other and play a minor role only in stabilizing the dimer interface. Each of the domains is constructed around a central, six-stranded, parallel β-sheet surrounded by α-helices. The α-domain and γ-domain have identical topologies, whereas the β-domain consists of a double Rossmann fold. There are two segments in each monomer where there is no observable electron density. These correspond to the N-terminal hexa-histidine tag derived from the expression vector plus the first 25 residues of the mature protein and to a surface polypeptide segment connecting the α- and β-domains (Asn-271 to Leu-276 in monomer A and Asn-271 to Thr-277 in monomer B).

Each dimer has two active sites centered upon the ThDP cofactor. The ThDP is bound at the dimer interface anchored to the protein by Mg^{2+} and adopts a V-shaped conformation, as is observed in our previous AHAS structure. This conformation is

TABLE I
Data collection and refinement statistics

Crystal data	
Unit cell length (Å)	$a = b = 153.98, c = 178.30$
Space group	$P422$
Crystal dimensions (mm)	$0.2 \times 0.2 \times 0.05$
Diffraction data[a]	
Temperature (K)	100
Resolution range (Å)	48.7–2.8
Observations $[I > 0\sigma(I)]$	571,130 (15,211)
Unique reflections $[I > 0\sigma(I)]$	52,457 (4,769)
Completeness (%)	97.8 (81.5)
R_{sym}[b]	0.091 (0.269)
$\langle I \rangle / \langle \sigma(I) \rangle$	10.4 (3.7)
Refinement	
Resolution limits (Å)	48.7–2.8
Number atoms per asymmetric unit	
Protein non-H	9,106
ThDP non-H	26
PPD[c] non-H	24
FAD non-H	2×53
CE non-H	2×27
Mg^{2+}	2
K^+	2
DTT[c]	2×8
Water molecules	832
R_{factor}	0.163
R_{free}	0.205
Root mean square deviations	
Bond lengths (Å)	0.006
Bond angles (°)	1.21
Ramachandran plot (%)	
Most favored	91.8
Additionally allowed	8.0
Generously allowed	0.2
Disallowed	0.0

[a] Values in parentheses are statistics for the 2.90–2.80 Å resolution shell.
[b] $R_{sym} = \Sigma |I - \langle I \rangle| / \Sigma \langle I \rangle$, where I is the intensity of an individual measurement of each reflection, and $\langle I \rangle$ is the mean intensity of that reflection.
[c] PPD, (4-{[(4′-amino-2′-methylpyrimidin-5′-yl)methyl]amino}pent-3-enyl diphosphate); DTT, dithiothreitol.

shaped by the side-chain of Met-525, which projects between the thiazolium and pyrimidine rings, forcing them to be oriented at an angle to one another. Two further stabilizing interactions are hydrogen bonds to the pyrimidine ring, from the backbone oxygen of Gly-523 to the 4′-amino group and from the side-chain of the catalytic glutamate (Glu-139) to N1′.

In monomer A, ThDP is missing the S1 and C2 atoms of the thiazolium ring. Loss of C2 from ThDP has been reported previously in the crystal structure of *Zymomonas mobilis* pyruvate decarboxylase (8). We suggest that formation of the product that we observe (4-{[(4′-amino-2′-methylpyrimidin-5′-yl)methyl]amino}pent-3-enyl diphosphate) results from reactions occurring as a result of the exposure of the crystal to high intensity radiation during synchrotron data collection. Groups containing sulfur are susceptible to this type of damage (26).

Each AHAS monomer contains 1 molecule of FAD. As mentioned earlier, the role of this cofactor is unclear because the AHAS reaction does not involve redox chemistry. FAD is in an extended conformation and interacts mostly with the β-domain with the flavin ring pointing toward the active site (Fig. 2). The overall structure and interactions of FAD remain largely unaltered in the AHAS·CE complex, compared with those in the free enzyme. The main change brought about by CE is that the flavin ring rotates away from CE (Fig. 2*b*) to avoid a steric clash between the C7 methyl of FAD and the methoxy carbon atom of the inhibitor. Superimposing monomer B of the AHAS·CE complex on to monomer B of the free AHAS structure (Fig. 2*b*) shows that the C7 methyl group of the flavin ring (which is at the extremity) moves by 2.5 Å. When monomer B of the AHAS·CE complex is superimposed on to monomer A of the free
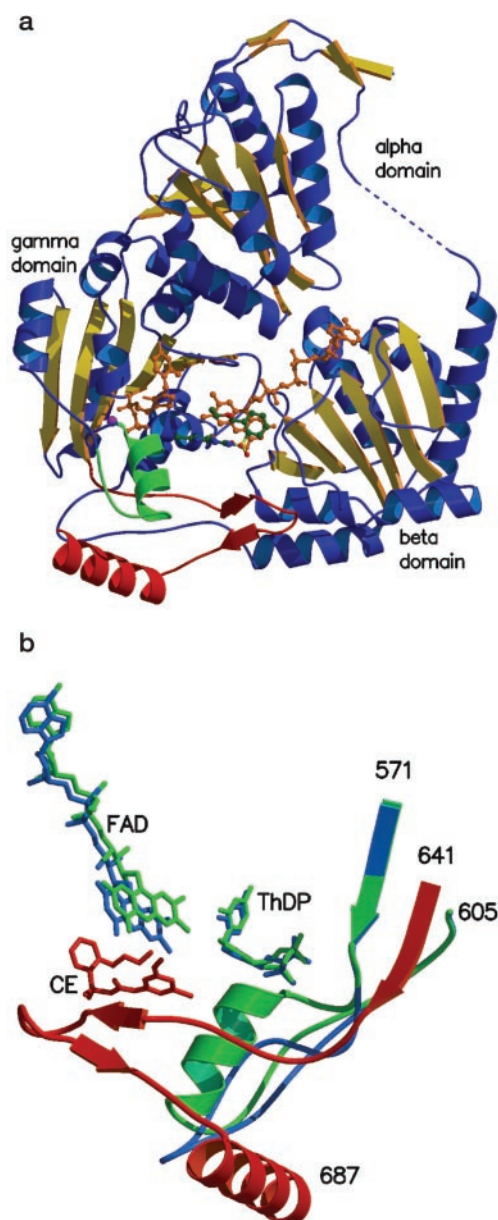
FIG. 2. *a*, structure of monomer B in the yeast AHAS·CE complex. The amino acid residues that are not observed in the structure of the free enzyme are colored *green* (the mobile loop) and *brown* (the C-terminal arm). ThDP and FAD are displayed as *tan-colored ball-and-stick models*. CE, the herbicidal inhibitor, is depicted as a *multicolored ball-and-stick model*. The connection between the α- and β-domains is shown partly as a *dashed line* to indicate that the region between Asn-271 and Thr-277 shows no observable electron density. *b*, major differences in the structure of yeast AHAS in the presence and absence of CE. The mobile loop region, FAD, and ThDP are shown in *green* (with CE) and *blue* (without CE). The C-terminal arm and CE are shown in *brown*.

AHAS, the movement of the C7 methyl of the flavin ring is even more pronounced, with the distance now 4.6 Å.

As mentioned above, Mg^{2+} anchors ThDP to the enzyme; the metal ion is coordinated to two phosphate oxygen atoms of the cofactor, the side-chain oxygen atoms of Asp-550 and Asn-577, the backbone oxygen of Gln-579, and 1 water molecule. This arrangement is similar to that found in other ThDP-dependent enzymes (6–9) but slightly different from that in the free enzyme (5), where the Gln-579 ligand is replaced by a water molecule. The displacement of the water in the present structure is brought about by a reorganization of residues 580–595, as described below. Each monomer contains a single K^+ at the
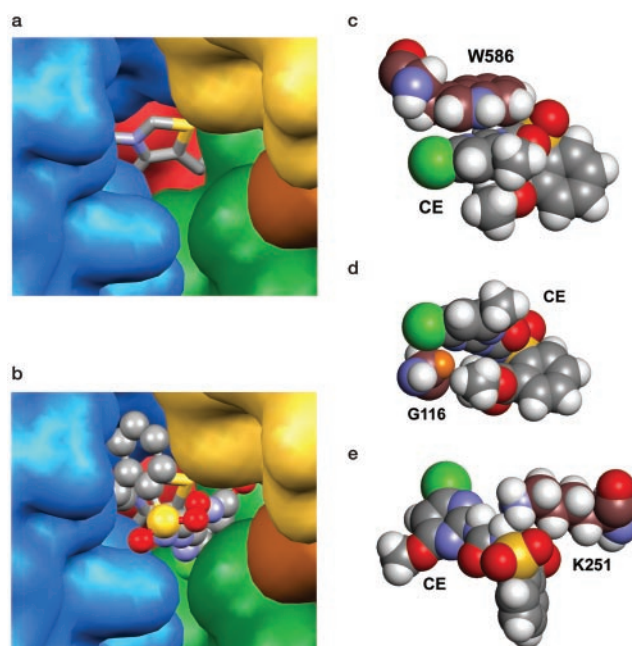

FIG. 3. *a*, the substrate access channel showing ThDP (*stick model*) at the bottom. *b*, the position of CE (*ball-and-stick model*) blocking the substrate access channel. Surfaces are colored *blue* (α-domain, monomer A), *yellow* (β-domain, monomer B), *red* (below ThDP, γ-domain, monomer B), *green* (mobile loop of the γ-domain, monomer B), and *brown* (C-terminal arm, monomer B). Interactions of CE with: *c*, Trp-586; *d*, Gly-116; and *e*, Lys-251. All atoms are shown as *space-filling balls* with amino acid carbon atoms colored *bronze*. The hydrogen atom that would be replaced if Gly-116 is mutated to other amino acids is shown in *orange*. For Trp-586, the more populated (68%) of the two alternate conformations is shown.

C-terminal end of an α-helix that leads away from the active site, as described previously (5). The yeast AHAS monomer contains only two cysteine residues, and one of these (Cys-357) is disulfide-linked to dithiothreitol that was present in the crystallization buffer. This nonconserved cysteine is far from the active site and is unlikely to have any functional importance.

Comparison with the AHAS Structure without CE—AHAS is a dimer in crystals of both the free enzyme (5) and in complex with CE. There are no major differences in the overall fold of both structures, with a root mean square deviation of 1.15 Å (1059 Cα atoms) when the dimeric structures are compared. However, there are two important changes that are observed in the complex. First, the three domains in the two monomers of AHAS are brought closer together in the complex, resulting in a reduction in the volume occupied by the active and herbicide-binding sites. Second, a capping region (Fig. 2*a*), which we define to consist of the 38 C-terminal amino acid residues 650–687 (the "C-terminal arm") and the polypeptide segment consisting of amino acid residues 580–595 (the "mobile loop"), becomes ordered, further restricting solvent accessibility to the active site. This capping region is involved in the formation of a substrate access channel that is missing in the previous uncomplexed enzyme structure. The substrate access channel is located at the dimer interface, and its inner face is formed by residues from all the three domains (Fig. 3*a*). The reaction center C2 atom of ThDP is positioned at the bottom of this channel, about 15 Å from the protein surface. In the structure without CE, the entire thiazolium ring of ThDP is solvent-accessible. As a result of the presence of the additional capping region in the current structure, most of ThDP is buried, and only the C2 atom of ThDP would be readily accessible to solvent.

As can be observed in Fig. 2, the C-terminal arm in the

Crystal Structure of an AHAS·Herbicide Complex

FIG. 4. **Stereoview depicting the conformation of CE when bound to yeast AHAS with the $2F_oF_e$ electron density shown.**
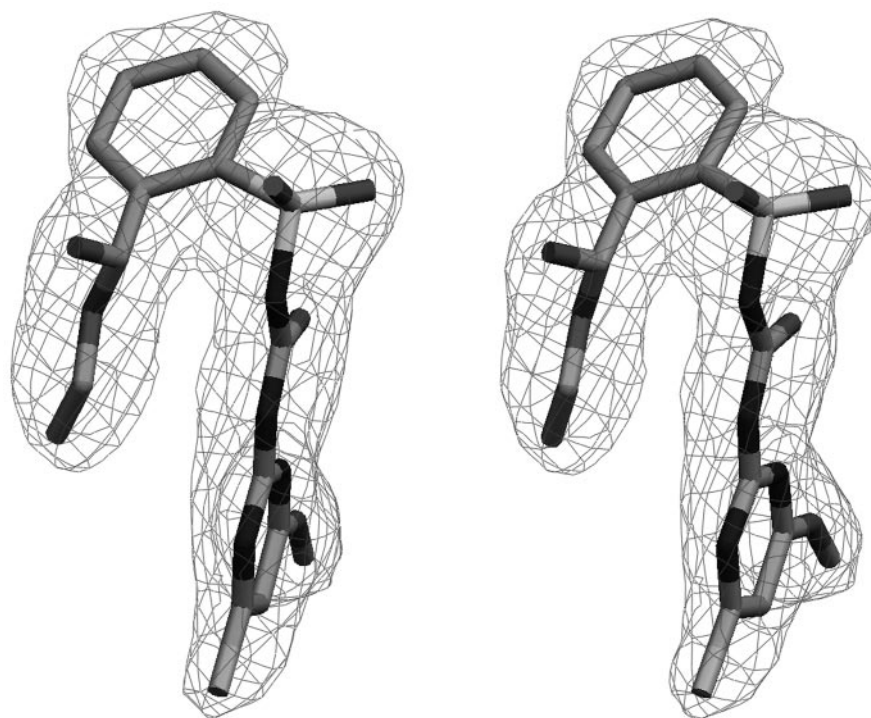
AHAS·CE complex adopts well-defined elements of secondary structure with residues 653–655 and 664–666 forming a small anti-parallel β-sheet, whereas the segment 669–683 forms an α-helix. As shown in Fig. 2a, residues 653–666 of this arm reach across from the γ-domain and attach to the β-domain. Phe-664 fits into a pocket on the surface of the β-domain that is bordered by Ala-358, Leu-362, and the aromatic ring of Tyr-458. A small polar surface on the tip of the arm forms stabilizing interactions between the arm and the β-domain, with an ion pair between Glu-663 and Lys-387, a hydrogen bond between Asp-662 and Gln-365, and a hydrogen bond between the carbonyl oxygen of Gly-658 and the side-chain of Asn-384. In addition, a series of van der Waals contacts involving Val-649, Val-651, Pro-653, Met-654, Val-655, Leu-661, and Phe-667 are made between the C-terminal arm and the β-domain. This feature, along with the enzyme-herbicide interactions, may provide an explanation for the overall tightening of the structure of the AHAS·CE complex. A further difference involves the mobile loop (residues 580–595); in the AHAS·CE complex, this region is organized into an α-helix (residues 580–589) and coil (residues 590–595) structure (Fig. 2b). In our previously published structure of yeast AHAS in the absence of CE (5), the entire mobile loop is completely disordered in one monomer but traceable as a random coil in the other (Fig. 2b). The corresponding region in related ThDP-dependent enzymes (6–9) is folded in an α-helix/coil structure closing over the active site, similar to that observed in the AHAS·CE complex. Apart from these major changes, some other differences are observed in the AHAS·CE complex, most notably the movement of the flavin ring of the FAD, mentioned previously, and also the conformation and position of the side-chains of Arg-380 and Met-354 have been altered significantly to optimize interactions with CE.

Two pieces of evidence suggest that the structural changes observed in the AHAS·CE complex are herbicide-induced and are not imposed by crystallization. First, attempts to co-crystallize AHAS and CE under the same conditions as the enzyme without CE were not successful. Similarly, conditions for crystallizing the complex do not yield crystals when the inhibitor is omitted. Second, diffraction data on existing crystals of AHAS soaked with CE (and other herbicidal inhibitors) do not show interpretable electron density for the herbicide.

The C-terminal arm does not have an equivalent in the closely related ThDP-dependent enzymes pyruvate oxidase, pyruvate decarboxylase, or benzoylformate decarboxylase. All have an α-helix near the C terminus, but none of them has the extended loop reaching across to interact with the β-domain. The extended loop structure may be related to another distinctive feature of AHAS: it is the only one of these four enzymes that possesses a regulatory subunit. The binding site for the regulatory subunit on AHAS has not been determined, but we speculate that the extended loop may form this binding site, possibly by acting as a clamp that wraps around the regulatory subunit.

Location and Conformation of CE—CE is bound in the substrate access channel of AHAS (Fig. 3b). An electron density map defining the conformation of CE is shown in Fig. 4. In contrast to the conventional extended conformation in which sulfonylureas are usually represented (Fig. 1a), CE is folded at the sulfonyl group with the two rings almost orthogonal to one another in two planes, with the ethyl side-chain extended parallel to the heterocyclic ring. The sulfonyl group and the attached aromatic ring are situated at the entrance to the substrate access channel, with the rest of the CE inserting into the channel (Fig. 3, *a* and *b*). Thus, CE completely blocks access to the active site, inhibiting AHAS by this mechanism.

CE is an extremely potent inhibitor of AHAS, with an inhibition constant in the low nanomolar range. The sulfonylurea-binding site is located at the dimer interface and is in the vicinity of the active site and the flavin ring of FAD. CE forms mainly hydrophobic contacts with the protein and FAD (Fig. 5), interacting with residues from both monomers and all three domains and with the C7 methyl group of FAD. In addition, the sulfonylurea bridge of the herbicide forms four hydrogen bonds with two amino acid residues Lys-251′ and Arg-380. Most of these contacts are with residues where mutation results in herbicide-resistant variants (see below). Two amino acids (Met-582 and Trp-586) within the mobile loop that are known
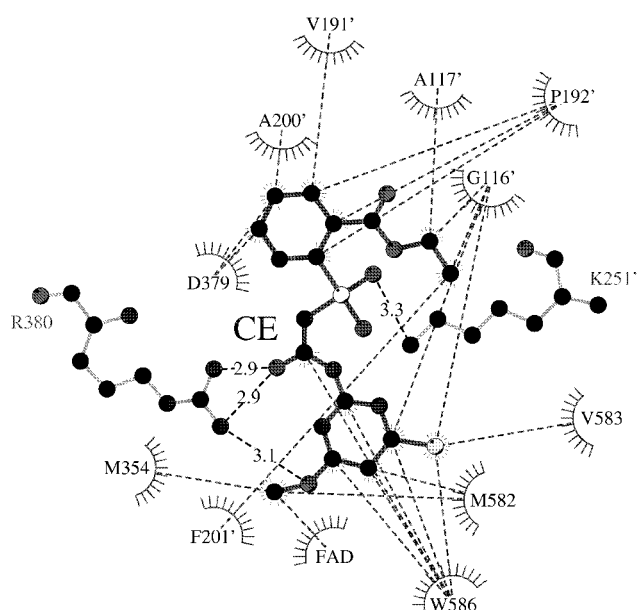
FIG. 5. **Interactions of CE with yeast AHAS.** Residues with and without the prime symbol (′) are derived from different monomers. *Broken lines* illustrate hydrophobic contacts and hydrogen bonds; for the latter, amino acid side-chains are shown with the lengths of the hydrogen bonds superimposed. The orientation of CE matches that shown in Fig. 1*a*.

FIG. 6. **The active site cavity of the yeast AHAS·CE complex.** Unoccupied space (after removal of a water molecule) is shown as *wiremesh*. The enamine/α-carbanion reaction intermediate that is formed after decarboxylation of the first molecule of pyruvate has been modeled into this cavity, with a stabilizing hydrogen bond to the 4′-amino of ThDP. CE and ThDP are at the *right* and *left*, respectively.

herbicide resistance sites exist in two conformations. Both residues are in direct contact with CE, and the alternate conformations of the side-chains are held in place by the bound herbicide.

Inhibition of AHAS by sulfonylureas is a time-dependent process (2, 10, 13). The initial inhibition that is observed immediately upon mixing the enzyme with substrate in the presence of these inhibitors becomes progressively stronger, taking tens of minutes to develop fully. This time dependence does not appear to be due to slow binding *per se* (2) because preincubation of the enzyme with sulfonylureas does not promote inhibition. It appears that ongoing catalysis is required for inhibition to develop, and this is consistent with the fact that inhibition is not competitive with the substrate (10, 27). This, in turn, leads to the suggestion (28) that sulfonylureas combine better with the enamine/α-carbanion reaction intermediate that is formed after decarboxylation of the first molecule of pyruvate. If this hypothesis is correct, then it follows that, in the AHAS·CE complex, there should be a cavity in the active site that would be able to accommodate the intermediate. Examination of the structure reveals the existence of such a cavity (Fig. 6) occupied by a single water molecule only. The intermediate can be modeled into the structure with no unfavorable interactions and a stabilizing hydrogen bond to the 4′-amino of ThDP. There is another consequence of the hypothesis that sulfonylureas combine better with the enzyme containing the enamine/α-carbanion reaction intermediate than with the enzyme at rest, the structure determined in the present report. To account for the stronger inhibition by sulfonylureas during AHAS catalysis, there should be additional interactions between the herbicide and the enzyme when it contains the reaction intermediate. To test this hypothesis experimentally would require crystallization of AHAS trapped as the reaction intermediate (or a close analog) together with the herbicide. The corresponding intermediate in transketolase has been trapped by adding a donor substrate that produces this complex while omitting the acceptor substrate that reacts with the intermediate (31). With AHAS, this strategy is not possible
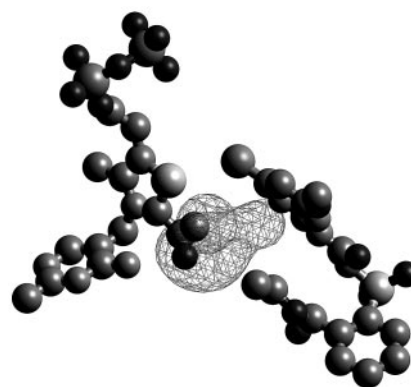
because pyruvate, the substrate required to generate the enamine/α-carbanion, is also the acceptor substrate with which it reacts.

Contacts with Herbicide Resistance Sites—Herbicide-resistant variants of AHAS have been identified in the enzyme from various microorganisms and plants. In yeast AHAS, mutations at 10 separate sites have each been shown to confer sulfonylurea insensitivity (29), and nine of these residues make direct, mainly hydrophobic, contacts with CE (Fig. 5). Only Phe-590 is not in direct contact with CE but this overlies Trp-586, which is locked into its two alternate conformations by being sandwiched between Phe-590 and the pyrimidine ring of CE. Other contacts to CE are with Val-191′, Phe-201′, Arg-380, and Met-582. Of these, the equivalent residues to both Val-191 and Met-582 have been shown to confer sulfonylurea resistance when mutated in *Escherichia coli* AHAS isoenzyme II (27, 30). The effect of mutation at Phe-201 and Arg-380 has not been tested to our knowledge.

Based on the structure of the AHAS·CE complex, it is easy to imagine how mutation of the contact residues might result in insensitivity to CE. We have constructed and performed detailed characterization of a series of herbicide-resistant AHAS mutants, and the results will be published elsewhere. Here we present some examples of AHAS mutations leading to sulfonylurea insensitivity. Mutations of Trp-586 are commonly identified in laboratory and field isolates, leading to strong resistance to sulfonylureas as well as to other classes of AHAS inhibitor. The mutation W586L in yeast AHAS results in a massive 6250-fold reduction in CE sensitivity. Our AHAS·CE structure shows that this amino acid is involved in ring-stacking interactions with the pyrimidine ring of CE (Fig. 3*c*). Mutation to a smaller and nonaromatic amino acid will greatly disrupt the interaction, consistent with the observed very large increase in the inhibition constant. Gly-116 lies between the pyrimidine ring and the ethyl side-chain (Fig. 3*d*), oriented so that any amino acid substitution would create steric clashes with CE unless there are compensating structural alterations of the protein. We have measured the apparent K_i of the yeast AHAS G116S mutant and shown that this variant is 1000-fold less sensitive to CE than the wild-type. A third example is Lys-251 (Fig. 3*e*); here the contact is a hydrogen bond between the side-chain amino group and one of the sulfonyl oxygen atoms. Substitution of Lys-251 by Thr, which would prevent this hydrogen bond from forming, results in 23-fold resistance to CE. The agreement between the enzyme structure (determined in the absence of substrate) and the effects of mutations on CE

inhibition (measured in the presence of substrate) suggests that the location and orientation of CE are not changed drastically during catalysis.

Binding of Other Herbicides—Yeast AHAS is inhibited by a range of sulfonylurea herbicides, with apparent K_i values ranging from 3.3 nM (CE) to 127 nM (chlorsulfuron). It is likely that each binds in a similar manner to CE, although this has yet to be verified experimentally. The binding of imidazolinone herbicides is more problematic, and these compounds are substantially weaker inhibitors than the sulfonylureas, with apparent K_i values in the 1–10 mM range. The considerable structural differences between the sulfonylureas (Fig. 1*a*) and the imidazolinones (Fig. 1*b*) make it unlikely that they would be able to form the same interactions, although we presume that both types of inhibitor bind in the substrate access channel. It is known that many AHAS mutations result in cross-resistance to both families of herbicide, but some are rather specific, resulting in resistance to one family of herbicides but not to the other. For example, P192S results in 65-fold resistance to CE but has no effect on imidazolinone sensitivity. Conversely, the mutation M354V has greater effects on imidazolinone sensitivity than CE sensitivity. Determination of the structure of yeast AHAS in complex with other sulfonylureas or imidazolinones will thus be of considerable interest.

REFERENCES

1. Shaner, D. L., Anderson, P. C., and Stidham, M. A. (1984) *Plant Physiol.* **76,** 545–546
2. LaRossa, R. A., and Schloss, J. V. (1984) *J. Biol. Chem.* **259,** 8753–8757
3. Chipman, D., Barak, Z., and Schloss, J. V. (1998) *Biochim. Biophys. Acta* **1385,** 401–419
4. Duggleby, R. G., and Pang, S. S. (2000) *J. Biochem. Mol. Biol.* **33,** 1–36
5. Pang, S. S., Duggleby, R. G., and Guddat, L. W. (2002) *J. Mol. Biol.* **317,** 249–262
6. Muller, Y. A., Schumacher, G., Rudolph, R., and Schulz, G. E. (1994) *J. Mol. Biol.* **237,** 315–335
7. Dyda, F., Furey, W., Swaminathan, S., Sax, M., Farrenkopf, B., and Jordan, F. (1993) *Biochemistry* **32,** 6165–6170
8. Dobritzsch, D., König, S., Schneider, G., and Lu, G. (1998) *J. Biol. Chem.* **273,** 20196–20204
9. Hasson, M. S., Muscate, A., McLeish, M. J., Polovnikova, L. S., Gerlt, J. A., Kenyon, G. L., Petsko, G. A., and Ringe, D. (1998) *Biochemistry* **37,** 9918–9930
10. Schloss, J. V., Ciskanik, L. M., and Van Dyk, D. E. (1988) *Nature* **331,** 360–362
11. Durner, J., and Böger, P. (1991) *Plant Physiol.* **95,** 1144–1149
12. Hill, C. M., Pang, S. S., and Duggleby, R. G. (1997) *Biochem. J.* **327,** 891–898
13. Chang, A. K., and Duggleby, R. G. (1997) *Biochem. J.* **327,** 161–169
14. Pang, S. S., and Duggleby, R. G. (1999) *Biochemistry* **38,** 5222–5231
15. Otwinowski, Z., and Minor, W. (1997) *Methods Enzymol.* **276,** 307–326
16. Navaza, J. (1994) *Acta Crystallogr. Sect. A* **50,** 157–163
17. Brünger, A. T., Adams, P. D., Clore, G. M., DeLano, W. L., Gros, P., Grosse-Kunstleve, R. W., Jiang, J.-S., Kuszewski, J., Nilges, M., Pannu, N. S., Read, R. J., Rice, L. M., Simonson, T., and Warren, G. L. (1998) *Acta Crystallogr. Sect. D Biol. Crystallogr.* **54,** 905–921
18. Jones, T. A., Zou, J. Y., Cowan, S. W., and Kjeldgaard, M. (1991) *Acta Crystallogr. Sect. A* **47,** 110–119
19. Wallace, A. C., Laskowski, R. A., and Thornton, J. M. (1995) *Protein Eng.* **8,** 127–134
20. Evans, S. V. (1993) *J. Mol. Graph.* **11,** 134–138
21. Kraulis, P. J. (1991) *J. Appl. Crystallogr.* **24,** 946–950
22. Merritt, E. A., and Murphy, M. E. P. (1994) *Acta Crystallogr. Sect. D Biol. Crystallogr.* **50,** 869–873
23. Brøns-Poulsen, J., Petersen, N. E., Horder, M., and Kristiansen, K. (1998) *Mol. Cell Probes* **12,** 345–348
24. Pang, S. S., and Duggleby, R. G. (2001) *Biochem. J.* **357,** 749–757
25. Lee, Y.-T., and Duggleby, R. G. (2002) *FEBS Lett.* **512,** 180–184
26. Burmeister, W. P. (2000) *Acta Crystallogr. Sect. D Biol. Crystallogr.* **56,** 328–341
27. Hill, C. M., and Duggleby, R. G. (1998) *Biochem. J.* **335,** 653–661
28. Schloss, J. V., and Aulabaugh, A. (1988) in *Biosynthesis of Branched Chain Amino Acids* (Barak, Z., Chipman, D. M., and Schloss, J. V., eds), pp. 329–356, VCH Press, Weinheim, Germany
29. Falco, S. C., McDevitt, R. E., Chui, C.-F., Hartnett, M. E., Knowlton, S., Mauvais, C. J., Smith, J. K., and Mazur, B. J. (1989) *Dev. Ind. Microbiol.* **30,** 187–194
30. Ibdah, M., Bar-Ilan, A., Livnah, O., Schloss, J. V., Barak, Z., and Chipman, D. M. (1996) *Biochemistry* **35,** 16282–16291
31. Fiedler, E., Thorell, S., Sandalova, T., Golbik, R., Konig, S., and Schneider, G. (2002) *Proc. Natl. Acad. Sci. U. S. A.* **99,** 591–595

Molecular Basis of Sulfonylurea Herbicide Inhibition of Acetohydroxyacid Synthase

Siew Siew Pang, Luke W. Guddat and Ronald G. Duggleby

Access the most updated version of this article at doi: 10.1074/jbc.M211648200

Alerts:

- When this article is cited
- When a correction for this article is posted

Click here to choose from all of JBC's e-mail alerts

This article cites 30 references, 9 of which can be accessed free at
http://www.jbc.org/content/278/9/7639.full.html#ref-list-1